Electron-impact dissociation of CH^+ ions: Measurement of C^+ fragment ions

M. E. Bannister,* H. F. Krause, and C. R. Vane

Physics Division, Oak Ridge National Laboratory, Oak Ridge, Tennessee 37831-6372, USA

N. Djurić,† D. B. Popović, M. Stepanović, and G. H. Dunn

JILA, University of Colorado and National Institute of Standards and Technology, Boulder, Colorado 80309-0440, USA

Y.-S. Chung

Department of Physics, Chungnam National University, 305-764 Daejon, Korea

A. C. H. Smith

Department of Physics and Astronomy, University College London, London WC1E 6BT, United Kingdom

B. Wallbank

Department of Physics, St. Francis Xavier University, Antigonish, Nova Scotia, Canada B2G 2W5

Absolute cross sections for electron-impact dissociation of CH^+ producing C^+ fragment ions were measured in the 3–100 eV range using a crossed electron-ion beams technique with total uncertainties of about 10% near the cross-section peak. Although the measured energy dependence agrees well with two sets of storage ring measurements, the magnitude of the present results lies about 15–25 % below the other results at the cross-section peak near 40 eV. Below 10 eV, the present data tend to exceed the storage ring data, consistent with the presence of excited states in the CH^+ ion beam. For energies above 29 eV, the cross sections should also include contributions from dissociative ionization, though no clear onset of this channel is evident in any of the three sets of measured data.
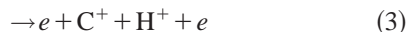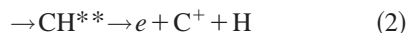
I. INTRODUCTION

Collisions of electrons with molecular ions play an important role in chemistry, particle and energy balance, and neutral transport in low-temperature plasma environments. In particular, hydrocarbon ions are found in the divertor and edge plasmas of fusion devices that use graphite for plasma-facing components [1] and may contribute to detachment of divertor plasmas through molecule assisted recombination [2]. They are also important in the chemistry of diffuse interstellar and planetary clouds [3] and in the plasma processing of diamond films [4,5]. Hence, cross sections for interactions of these molecular ions with electrons, atoms, and photons are vital for modeling and diagnosing these varied plasma environments.

The production of C^+ fragment ions by electron-impact dissociation of CH^+ ions can occur by a number of different channels:

$$e + CH^+ \rightarrow e + C^+ + H \tag{1}$$

$$\rightarrow CH^{**} \rightarrow e + C^+ + H \tag{2}$$

$$\rightarrow e + C^+ + H^+ + e \tag{3}$$

$$\rightarrow CH^{**} \rightarrow C^+ + H^-. \tag{4}$$

The first process, direct dissociative excitation (DDE), involves a vertical transition from the initial state of CH^+ to a dissociative excited state. The second process, resonant dissociative excitation (RDE), proceeds through the resonant capture of the incident electron to a Rydberg state of the neutral molecule CH^{**} which then decays by ejecting an electron and dissociating. Hereafter, we will refer to the first two processes together as simply dissociative excitation (DE). Dissociative ionization (DI), the third process, is similar to DDE but ends in a dissociative state with two ion fragments. The last process producing C^+ fragments, resonant ion pair (RIP) formation, is expected to be negligible compared to the DE and DI contributions, based on RIP measurements on other systems [6–8].

The electron-impact dissociation of CH^+ and CD^+ in the DE and DI channels has been investigated previously using several techniques. Amitay *et al.* [9] measured the production of C^+ ions up to 40 eV at the Heidelberg Test Storage Ring (TSR), but their results had total absolute uncertainties of about 50% due to difficulties in measuring the ion current circulating in the storage ring. Forck [10] investigated the dissociation of CD^+ at TSR, measuring cross sections for production of C^+ ions as well as C and D neutrals, also with total uncertainties of about 50%. Djurić *et al.* [11] measured the sum of DE and DI for the H^+/D^+ production channel using a crossed-beam technique; below the DI threshold where DE provides the only energetically allowed channel, their results for the production of D^+ were in excellent

___

*Electronic address: bannisterme@ornl.gov

†Present address: Jet Propulsion Laboratory, 4800 Oak Grove Drive, Pasadena, CA 91109, USA.
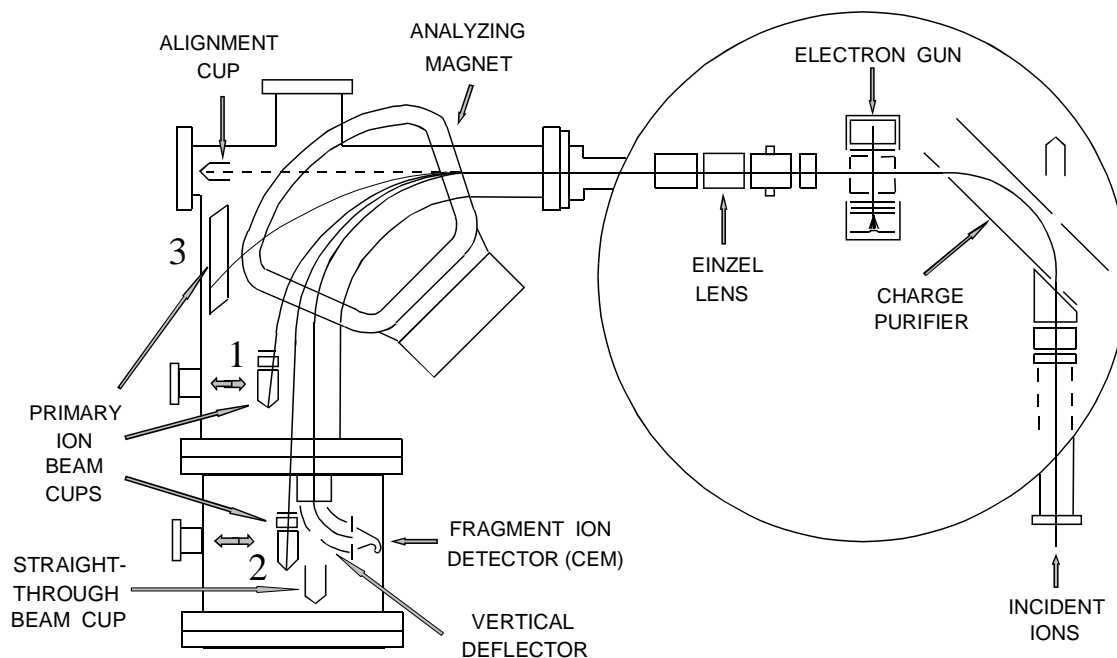
FIG. 1. Electron-ion crossed-beams experimental apparatus. See text for an explanation. The fragment ion detector and vertical deflector are rotated 90° to the plane of the figure.

agreement with those of Forck [10] for the production of C neutrals. Janev and Reiter [12] have recently published a review of data for collisions of simple hydrocarbon ions and neutrals with electrons and protons, including empirical formulas for electron-impact DE and DI of CH^+, along with information about the thresholds and average kinetic energies of release (KERs) for these processes.

The measurements reported here are absolute total cross sections for the production of C^+ ions by electron-impact on CH^+. The measurements were performed using the ORNL electron-ion crossed beams apparatus [13,14] with CH^+ ions produced in a Caprice electron-cyclotron-resonance (ECR) ion source. Dissociation cross sections measured for H_3O^+ and D_3O^+ ions using this apparatus have been reported [15] for heavy-fragment ion channels. The present results are compared with the measurements of Forck [10] and Amitay *et al.* [9] as well as the analytical fits of Janev and Reiter [12].

II. EXPERIMENT

The electron-ion crossed-beams apparatus used for the present study has been described in detail previously [13,14], but changes since the latter of these publications and issues specific to measurements of cross sections for dissociation of molecular ions will be discussed below. The apparatus is shown schematically in Fig. 1.

A. Ion and electron beams

The CH^+ molecular ions were produced in the ORNL ECR ion source [16] using methane as a source gas. The ions were extracted at 10 kV and mass selected with magnetic analysis. Mass spectra of extracted ions demonstrated that

the only impurity ions in the analyzed beam were $^{13}C^+$ ions, comprising less than 1% of the extracted ions with $m/q = 13$ as estimated from the $^{12}C^+$ peak and known natural abundances. Since the lifetimes of electronic and rovibronic excited states of CH^+ [17,18] are much longer than the 1 μs flight time of the ions from the ECR source to the collision volume, the excited state population of the target CH^+ ions is essentially preserved from the ion source. Even operating the source at minimal microwave power levels of a few watts and with source pressures of order 10^{-6} Torr, the electron temperature in the ECR discharge may be tens of electron volt or more, producing a sizable fraction of CH^+ ions in excited states, including higher vibrational levels of the $X^1\Sigma$ ground state and the $a^3\Pi$ metastable state. Because the $a^3\Pi$ state has a lifetime of approximately 7 s [17], it was not feasible to measure the population of these ions in the beam extracted from the ECR source. The presence of excited states has been found to have a significant effect on measured cross sections for the dissociative recombination of CH^+ [17,19], although less dramatic influences are expected for DE and DI. Potential-energy curves for the lowest six states of CH^+ are shown in Fig. 2 [17,20–24] along with their separated atom asymptotes.

The ions are transported with magnetic and electrostatic optics from the ECR ion source to the crossed-beams apparatus. Just before the collision volume the ions are deflected electrostatically through 90° in a charge purifier to eliminate any charge-exchange components in the beam. In the collision volume, the ion beam (1 mm diameter) interacts at right angle with an electron beam formed by a magnetically confined gun described below. Upon leaving this interaction region, the parent and fragment ions are separated by a double focusing 90° sector analyzing magnet with a radius of cur-
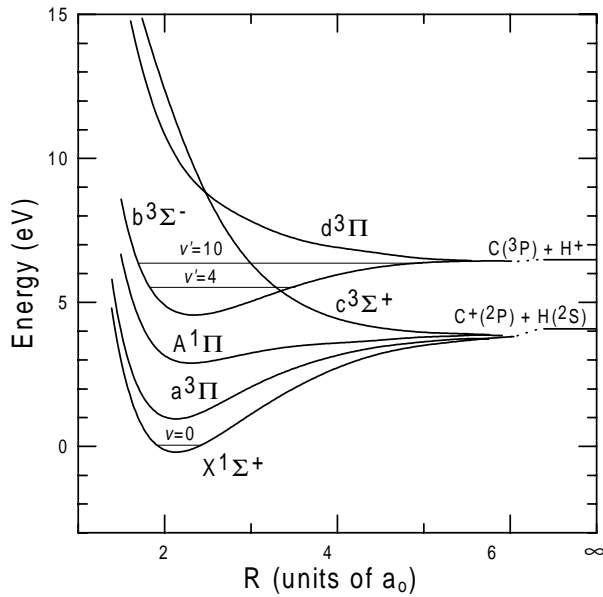
FIG. 2. Potential energy curves for CH$^+$. Solid curves are data from Refs. [16–20] shown with their separated atom limits and zero energy taken as the $v=0$ level of the $X^1\Sigma^+$ ground state. The vibrational levels of the $b^3\Sigma^-$ state were calculated using the spectroscopic constants of Ref. [23].

vature of 20 cm. This ensures that the collision volume is imaged at the throat of the fragment ion detector. The C$^+$ product ions are deflected 90° by the magnet, then electrostatically deflected out of the magnetic dispersion plane and onto a 1.0 cm diameter channel electron multiplier (CEM). The CH$^+$ primary ions are deflected less by the analyzing magnetic field and collected in Faraday cup 2, which is closest to the fragment ion detector (see Fig. 1). The postcollision Einzel lens shown in Fig. 1 was grounded in the present study.

The electron gun used for the present study is a magnetically confined model described previously [14,25,26]. A magnetic field of 250 G confines the electrons and yields a uniform rectangular cross section (approximately 2 mm wide by 10 mm high) over the 2 mm length of the interaction region. Spiraling of the electrons is minimized [26] by accelerating them in a uniform electric field through a series of apertures between the indirectly heated planar cathode and the collision volume. The electron collector comprises a stack of tantalum "razor blades" turned with the sharp edges facing the interaction region; this design helps prevent backscattered electrons from returning to the collision volume. The collector is also biased +300 V with a battery to minimize the escape of secondary electrons. Typical electron currents are 11 μA at 10 eV and 230 μA at 100 eV. The electrons are chopped at 1 kHz in order to separate the dissociation signal from the relatively larger background count rate associated with the ion beam. Measurements of excitation cross sections using the configuration shown in Fig. 1 [27] indicated that the net collision energy distribution is degraded from 0.4 eV of the gun [25,26] to about 1.5 eV full-width-half-maximum as a result of field leakage into the collision region from the postcollision ion deflector plates.

The overlap of the ion and electron beams in the direction perpendicular to both beams (vertical direction) was measured with a slit probe moving through the center of the interaction region. Current profiles of the ion and electrons, $I_i(z)$ and $I_e(z)$, were measured independently and numerical integration yielded the form factor F needed for determination of absolute cross sections

$$F = \frac{\int I_e(z)dz \int I_i(z)dz}{\int I_e(z)I_i(z)dz}. \quad (5)$$

B. Cross section determination and uncertainties

The absolute cross sections are determined [28] from measured quantities using

$$\sigma(E) = \frac{R}{I_iI_e} \frac{qe^2v_iv_e}{\sqrt{v_i^2+v_e^2}} \frac{F}{\epsilon}, \quad (6)$$

where $\sigma(E)$ is the absolute cross section at the center-of-mass electron-impact energy E, R is the fragment signal rate, I_i and I_e are the incident ion and electron currents, respectively, qe is the charge of the incident ions, v_i and v_e are the incident ion and electron velocities, respectively, F is the form factor that is determined from the two beam profiles, and ϵ is the channeltron detection efficiency for the product ions that we estimated to be 98% [29].

The systematic uncertainties in the experiment arise from a number of sources connected to the measurement of the quantities in Eq. (6) and are given at a level equivalent to 90% confidence level for statistical uncertainties. The largest contribution is from the detection of the C$^+$ fragment ions (estimated at 5%); this includes detection efficiency ϵ, signal pulse transmission and discrimination, and dead times of the detector and signal processing electronics. The transmission and collection of the fragment ions contributes an estimated 4% and includes possible losses due to fragment ions in the tail of the KER distribution. These first two uncertainties are connected to the measurement of the true signal rate (R/ϵ) in Eq. (6). The systematic uncertainty of measuring the absolute form factor F is estimated to be 4%. Other contributions are from determinations of the ion current (3% including beam impurities), electron current (2%), and the ion and electron velocities (1% each). The quadrature sum of all these contributions is ±8.5%. Combining this sum with the statistical uncertainties at a 90% confidence level yields the total expanded uncertainties for the measurements, typically about 10% near the cross-section peak.

C. Diagnostics

Upon dissociation of a molecular ion, the fragments share KER that is the result of redistribution of the excess internal energy in the molecular ion after the collision with an electron. Thus, a given fragment will have a velocity the vector sum of that of the target ion and a velocity component due to its share of the KER. The maximum change in lab frame
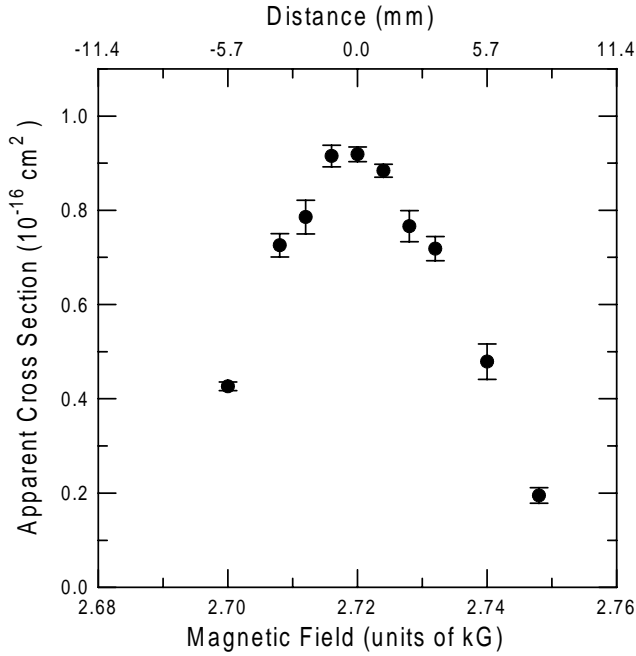
FIG. 3. Apparent dissociation cross sections as a function of the analyzing magnetic field. Measurements were made at a center-of-mass energy of 100 eV and the error bars represent one standard deviation relative uncertainties.

momentum occurs when the corresponding additional momentum Δp is parallel or antiparallel to the incident ion momentum P_0. In this case the dispersion of the fragment ion by the analyzing magnet causes a horizontal displacement Δx at the detector which is given by

$$\Delta x = D r_0 \ \frac{\Delta p}{p_0}, \tag{7}$$

where $p_0 = (m/M)P_0$ is the fragment momentum for zero KER with parent and fragment masses M and m, respectively, r_0 is the radius of curvature of the analyzing magnet, and D is the dispersion coefficient. For the present configuration, a double-focusing 90° sector magnet with entrance and exit angles of 26.5° and image and object distances of $2r_0$, the dispersion coefficient is 4 [30]. Applying conservation of energy and momentum to the fragmentation process, one finds that the maximum horizontal displacement is

$$\Delta x_{max} = 4 r_0 \left(\frac{\Delta E}{E_i} \frac{M-m}{m} \right)^{1/2}, \tag{8}$$

where ΔE is the KER and E_i is the energy of the incident (parent) ion.

Measurements of the apparent dissociation cross section at a center-of-mass energy of 100 eV as a function of the analyzing magnetic field are shown in Fig. 3. The axis at the top of Fig. 3 indicates the distance that the center of the fragment ion peak is moved from the center of the detector by the analyzing magnetic field. The fragment ion peak can be moved 1.2 mm in either direction without any loss of apparent signal from the detector. At 5.7 mm in either direc-

tion, one-half of the apparent signal is lost from the detector. From these two observations and noting that the radius of the CEM is 5.0 mm, one can infer that essentially all the signal is collected by the detector for a magnetic field of 2.72 kG and the maximum displacement Δx_{max} of the fragment ions from the center of the detector due to the effects of KER is 4.5 mm. Thus, an upper limit can be estimated for the average KER for dissociation of the CH^+ target ions by using Eq. (8). Noting that $r_0 = 20$ cm for our analyzing magnet, one obtains an upper limit of 3.8 eV for the average KER.

The KER also causes angular spreading of the fragment ions, but this is mostly compensated for by the double-focusing analyzer magnet. As demonstrated by trajectory modeling using the computer program SIMION [31], the spread of the C^+ fragment ions at the detector due to KER perpendicular to the target ion velocity is much smaller than that due to KER in the parallel direction. Note that angular effects of KER are sufficient, however, to cause significant loss of H^+ fragment ions, which are not collected in this experiment.

The voltage applied to the final vertical deflector that directs the C^+ fragment ions onto the CEM was also scanned to test sensitivity and centering of C^+ ions steered in this element. The apparent cross section did not change for several hundred volts on either side of the value (8.5 kV) used for taking the present data.

The high background count rates of 5–6 kHz/nA due to dissociation of the CH^+ ions on residual gas in the collision volume necessitated limiting the incident ion current. By measuring the apparent cross section as a function of the total detector count rate, it was found that full signal could be maintained with count rates of 70 kHz, but increasing it beyond 100 kHz caused a reduction of greater than 10% due to reduced gain of the detector. Lowering the total count rate further, to below 20 kHz, did not yield any increase in the apparent cross section. Hence, most of the present data were taken with ion currents of 10–12 nA and count rates in the 50–70 kHz range to minimize the time needed to reach a given statistical precision in the data while maintaining detector gain and limiting dead-time corrections of the electronics to less than 7%.

The position of the Faraday cup that collected the primary ion beam was optimized to maintain the full current and signal while minimizing the ion background on the detector. Parameters for the electron chopping such as frequency, voltage, and delay times were also varied and found to have a negligible effect on the measured cross sections.

III. RESULTS

Absolute cross sections for electron-impact dissociation of CH^+ ions producing the C^+ fragment for energies up to 100 eV are shown in Fig. 4. The present measurements, the sum of the DE and DI channels, are indicated as filled circles and are shown with one standard deviation relative error bars, except for the point at 60 eV, where the outer set of error bars represents the total uncertainty of about 10%. The upper and lower solid curves represent the storage ring mea-
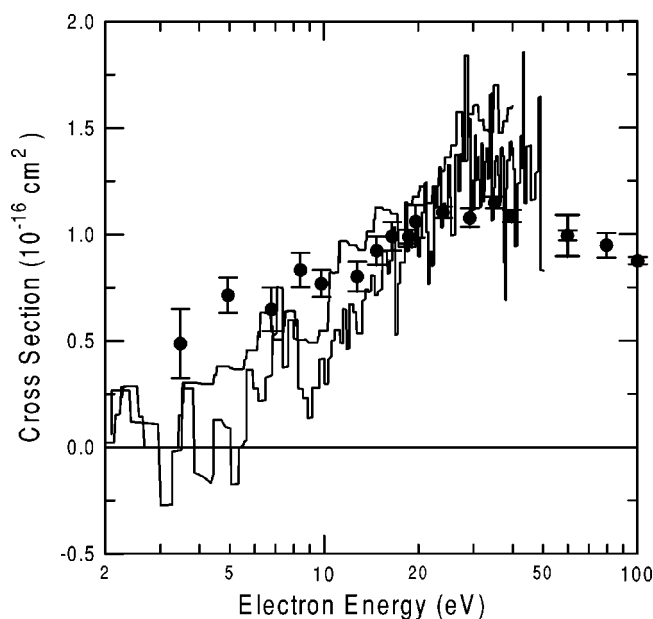
FIG. 4. Absolute cross sections for the production of C$^+$ fragment ions by electron-impact dissociation of CH$^+$ ions as a function of center-of-mass energy. The filled circles are the present measurements shown with one standard deviation relative error bars. The outer error bar at 60 eV represents the total uncertainty at a 90% confidence level. The upper and lower solid curves represent the storage ring measurements of Refs. [9] and [10], respectively.

surements of Amitay *et al.* [9] and Forck [10], respectively, for production of C$^+$ ions.

For energies above 15 eV, the energy dependence of the storage ring measurements [9,10] is similar to that of the present results, but the magnitudes of Forck [10] and of Amitay *et al.* [9] lie about 15–25 % above the present value for the peak of the cross section near 40 eV. Considering the large total uncertainty of the earlier data, estimated at 50%, those data are in agreement with the present results. For energies less than 15 eV, however, the present cross sections tend to remain high as one approaches the dissociation energy of 4.08 eV for ground-state ions, which is consistent with the presence of excited states in the CH$^+$ ion beam produced in the ECR ion source for our experiment. The ion source used at TSR for the work of Forck and Amitay *et al.* produced an estimated 60–70 % of CH$^+$ ions in the $a\,^3\Pi$ metastable state, although after storing the ions for 10–20 s, the estimated population was only 5–10 % of the total ion current during the cross-section measurements. The population of the $a\,^3\Pi$ metastable state could be much higher than 5–10 % in the present experiment, and higher rovibrational levels within the $a\,^3\Pi$ state may also be populated.

The measured cross section is nonzero below the thresholds for vertical transitions from the $X\,^1\Sigma$ ground and $a\,^3\Pi$ metastable states at 9.7 eV and 8.6 eV, respectively, suggesting that RDE plays a role in dissociation in the low-energy region. However, one should note that the vertical transition thresholds for the $X\,^1\Sigma$ and $a\,^3\Pi$ states will be lowered by the presence of ions in higher v levels. Another mechanism that may contribute at these energies is the dissociation of the

$b\,^3\Sigma^-$ state into the $c\,^3\Sigma^+$ repulsive state following a vertical transition from the $a\,^3\Pi$ state (see Fig. 2). This process would require excitation to the $v=4$ to $v=10$ levels [23] of $b\,^3\Sigma^-$ in order to reach the $c\,^3\Sigma^+$ dissociative state and would yield KERs in the range of 1.4–2.5 eV, consistent with the upper limit of 3.8 eV deduced from Fig. 3 and Eq. (8). The opening of this channel would occur at about 2–5 eV, depending on the rovibrational level of the initial $a\,^3\Pi$ state molecular ion. Although this pathway is also open from the ground state, the cross section for excitation to the $b\,^3\Sigma^-$ state should be smaller from the $X\,^1\Sigma$ ground state than from the $a\,^3\Pi$ metastable state since the singlet-triplet transition would require a spin flip.

The empirical cross sections of Janev and Reiter [12] exceed the present data by a factor of 2–4 below 20 eV, suggesting they have overestimated the contribution of RDE for this collision system. Likewise, their sum of DE (DDE and RDE) plus DI exceeds the present measurements by a factor of almost 2 at 100 eV. Perhaps the present data along with the storage ring results can be used to refine their empirical fits, particularly the relative contributions of RDE and DDE as well as the ratio of the C$^+$ and H$^+$ fragment channels for DE of CH$^+$.

Above the DI threshold of 29 eV [32] the present measurements are the sum of the DE and DI channels producing C$^+$ fragment ions, although no clear onset of the DI contribution can be seen in Fig. 4 for any of the three data sets.

IV. CONCLUSIONS

Absolute cross sections for electron-impact dissociation of CH$^+$ ions producing C$^+$ fragment ions have been measured with the ORNL crossed-beams apparatus with a total expanded uncertainty of approximately 10% near the peak. The storage ring measurements of Forck [10] and Amitay *et al.* [9] are about 15–25 % higher than the present results, but the discrepancy is within the combined experimental uncertainties. The low-energy behavior of the present data suggests a significant population of target CH$^+$ ions in excited states, both electronic and vibrational, as expected for an ECR ion source. The dispersion pattern of the C$^+$ fragment ions in the analyzing magnetic field yields an estimated upper limit of 3.8 eV for the average KER. Future investigations will include CH$^+$ ions produced by a cooler ion source in order to study the influence of excited states, both on the cross section and the KER.

[1] H. Tawara, in *Atomic and Molecular Processes in Fusion Plasmas*, edited by R. K. Janev (Plenum, New York, 1995), pp. 461–496.

[2] R.K. Janev, T. Kato, and J.G. Wang, Phys. Plasmas **7**, 4364 (2000).

[3] A. Dalgarno, in *Atomic Processes and Applications*, edited by P.G. Burke and B.L. Moiseiwitsch (North-Holland, Amsterdam, 1976), pp. 109–132.

[4] J. Luque, W. Juchmann, E.A. Brinkman, and J.B. Jeffries, J. Vac. Sci. Technol. A **16**, 397 (1998).

[5] X.D. Zhu, R.J. Zhan, H.Y. Zhou, X.H. Wen, and D. Li, J. Vac. Sci. Technol. A **20**, 941 (2002).

[6] W. Zong, G.H. Dunn, N. Djurić, M. Larsson, C.H. Greene, A. Al-Khalili, A. Neau, A.M. Derkatch, L. Vikor, W. Shi, A. Le Padellec, S. Rosén, H. Danared, and M. af Ugglas, Phys. Rev. Lett. **83**, 951 (1999).

[7] A. Le Padellec, N. Djurić, A. Al-Khalili, H. Danared, A.M. Derkatch, A. Neau, D.B. Popović, S. Rosén, J. Semaniak, R. Thomas, M. af Ugglas, W. Zong, and M. Larsson, Phys. Rev. A **64**, 012702 (2001).

[8] N. Djurić, G.H. Dunn, A. Al-Khalili, A.M. Derkatch, A. Neau, S. Rosén, W. Shi, L. Vikor, W. Zong, M. Larsson, A. Le Padellec, H. Danared, and M. af Ugglas, Phys. Rev. A **64**, 022713 (2001).

[9] Z. Amitay, D. Zajfman, P. Forck, U. Hechtfischer, M. Grieser, D. Habs, D. Schwalm, and A. Wolf, in *Applications of Accelerators in Research and Industry*, edited by J.L. Duggan and I.L. Morgan (AIP Press, New York, 1997), p. 51.

[10] P. Forck, Ph.D. thesis, Ruprecht-Karls-Universität Heidelberg, 1994 (unpublished).

[11] N. Djurić, Y.-S. Chung, B. Wallbank, and G.H. Dunn, Phys. Rev. A **56**, 2887 (1997).

[12] R.K. Janev and D. Reiter, Phys. Plasmas **9**, 4071 (2002).

[13] M.E. Bannister, Phys. Rev. A **54**, 1435 (1996).

[14] D.C. Gregory, F.W. Meyer, A. Müller, and P. Defrance, Phys. Rev. A **34**, 3657 (1986).

[15] P.A. Schulz, D.C. Gregory, F.W. Meyer, and R.A. Phaneuf, J. Chem. Phys. **85**, 3386 (1986).

[16] F. W. Meyer, in *Trapping Highly Charged Ions: Fundamentals and Applications*, edited by J. Gillaspy (Nova Science, Huntington, NY, 2001), p. 117.

[17] Z. Amitay, D. Zajfman, P. Forck, U. Hechtfischer, B. Seidel, M. Grieser, D. Habs, R. Repnow, D. Schwalm, and A. Wolf, Phys. Rev. A **54**, 4032 (1996).

[18] F.R. Ornellas and F.B.C. Machado, J. Chem. Phys. **84**, 1296 (1986).

[19] P.M. Mul, J.B.A. Mitchell, V.S. D'Angelo, P. Defrance, J.W. McGowan, and H.R. Froelich, J. Phys. B **14**, 1353 (1981).

[20] S. Green, P.S. Bagus, B. Liu, A.D. McLean, and M. Yoshimine, Phys. Rev. A **5**, 1614 (1972).

[21] I. Kusunoki, S. Sakai, S. Kato, and K. Morokuma, J. Chem. Phys. **72**, 6813 (1980).

[22] R.P. Saxon, K. Kirby, and B. Liu, J. Chem. Phys. **73**, 1873 (1980).

[23] R.P. Saxon and B. Liu, J. Chem. Phys. **78**, 1344 (1983).

[24] B. Levy, J. Ridard, and E. Le Coarer, Chem. Phys. **92**, 295 (1985).

[25] P.A. Taylor and G.H. Dunn, Phys. Rev. A **8**, 2304 (1973).

[26] P.A. Taylor, K.T. Dolder, W.E. Kauppila, and G.H. Dunn, Rev. Sci. Instrum. **45**, 538 (1974).

[27] D.S. Belić, R.A. Falk, G.H. Dunn, D. Gregory, C. Cisneros, and D.H. Crandall, Bull. Am. Phys. Soc. **27**, 49 (1981).

[28] See, for example, M.F.A. Harrison, Br. J. Appl. Phys. **17**, 371 (1966).

[29] D.C. Gregory, P.F. Dittner, and D.H. Crandall, Phys. Rev. A **27**, 724 (1983).

[30] H. A. Enge, in *Focusing of Charged Particles*, edited by A. Septier (Academic Press, Orlando, 1967), Vol. II, Chap. 4.2, pp. 203–264.

[31] SIMION 3D, Version 6.0, David Dahl, INEL-95/0403 (1995).

[32] H.M. Rosenstock, K. Draxl, B.M. Steiner, and J.T. Herron, J. Phys. Chem. Ref. Data **6**, 1 (1977).